International Journal of Heat and Mass Transfer 82 (2015) 250–258

Contents lists available at ScienceDirect

International Journal of Heat and Mass Transfer

journal homepage: www.elsevier.com/locate/ijhmt

Anisotropic thermal transport in MOF-5 composites

Yang Ming [a], Hang Chi [a], Rachel Blaser [c], Chunchuan Xu [c], Jun Yang [c], Mike Veenstra [c], Manuela Gaab [d], Ulrich Müller [d], Ctirad Uher [a], Donald J. Siegel [b,*]

[a] Department of Physics, University of Michigan, 1440 Randall Lab, 450 Church St., Ann Arbor, MI 48109-1040, USA
[b] Mechanical Engineering Department, University of Michigan, 2250 G. G. Brown Laboratory, 2350 Hayward St., Ann Arbor, MI 48109-2125, USA
[c] Ford Motor Company, Research and Advanced Engineering, MD 1170/RIC, P.O. Box 2053, Dearborn, MI 48121, USA
[d] BASF SE, Process Research and Chemical Engineering, 67056 Ludwigshafen, Germany

ARTICLE INFO

Article history:
Received 7 June 2014
Received in revised form 17 October 2014
Accepted 13 November 2014

Keywords:
Metal-organic frameworks
Anisotropic transport
Thermal conductivity
Hydrogen storage
Microstructure-sensitive processing

ABSTRACT

Metal-organic frameworks (MOFs) are a new class of porous, crystalline materials with applications in the capture, storage, and separation of gasses. Although much effort has been devoted to understanding the properties of MOFs in powder form, in a realistic system the MOF media will likely be employed as dense compacts, such as pucks or pellets, to maximize volumetric efficiency. In these applications efficient transport of the heat of adsorption/desorption is an important design consideration. Consequently, densified composites consisting of a physical mixture of a MOF and expanded natural graphite (ENG) have been proposed as a means to enhance the intrinsically low thermal conductivity of these materials. Here we demonstrate that the high-aspect ratio of ENG particles, combined with uni-axial compression, results in anisotropic microstructural and thermal transport properties in composite MOF-5/ENG pellets. Microscopy of pellet cross-sections revealed a textured microstructure with MOF particle boundaries and ENG orientations aligned perpendicular to the pressing direction. This anisotropy is manifested in the thermal conductivity, which is two to four times higher in directions perpendicular to the pressing direction. We further demonstrate that this anisotropy can be exploited using two processing techniques. First, a custom die and densification process allows for reorientation of the preferred heat flow pathway. Second, a layered MOF-5/ENG microstructure increases the thermal conductivity by an order of magnitude, with only minor ENG additions (5 wt.%). These results reveal that anisotropic thermal transport in MOF composites can be tailored using a judicious combination of second phase additions and processing techniques.

1. Introduction

Metal-organic frameworks (MOFs) are porous, crystalline materials comprised of metal–oxygen clusters connected by organic linkers [1]. The high surface area, building-block-like synthesis procedure, and permanent porosity of MOFs make them attractive candidates for applications such as gas storage, gas separations, and catalysis [2–4]. For example, MOFs have demonstrated record-setting storage capacities for alternative transportation fuels such as hydrogen [5] and natural gas [6], and are also being explored for carbon capture applications [7].

While MOF attributes such as surface area and pore volume play an important role in determining their gas storage capacity, thermal transport properties should also be considered. For example, in gas storage applications requiring rapid uptake (e.g., refueling of a vehicle), the exothermic heat of adsorption [8,9] should be expelled in an efficient fashion in order to maximize performance. As higher temperatures reduce storage capacity, the inclusion of a heat-exchanging manifold within the storage vessel has been explored to enhance heat removal [10]. For adsorbents having low thermal conductivities the demands placed upon heat exchanger increase, typically at the expense of reduced volumetric and gravimetric storage density (due to additional mass and volume associated with the heat-exchanging manifold), and potentially higher cost. An alternative to an elaborate heat exchanger is to increase the thermal conductivity of the adsorbent medium itself.

Unfortunately, the thermal transport behavior of MOFs has received relatively little attention [9,11–15]. Huang et al. predicted the thermal conductivity of single crystal MOF-5 to be 0.31 W/m K at 300 K using molecular dynamics simulations [11]. Experimental measurements on single crystals of the same MOF were also

* Corresponding author.
E-mail address: djsiege@umich.edu (D.J. Siegel).

http://dx.doi.org/10.1016/j.ijheatmasstransfer.2014.11.053
0017-9310/

reported over a temperature range of 6 to 300 K, with a value 0.32 W/m K measured at 300 K [12]. In addition to these single crystal studies, Liu et al. [13] reported that the thermal conductivity of MOF-5 powders could be increased via compression/pelletization and through combination with high-conductivity additives such as expanded natural graphite (ENG), which has a thermal conductivity of ~150 W/m K [16]. For example, in pellets densified to 0.5 g/cm^3 the addition of 10 wt.% ENG resulted in a factor of five improvement in thermal conductivity (0.56 W/m K at 298 K) relative to neat MOF-5 pellets at the same density (0.10 W/m K). Compaction alone also improves thermal conductivity, but to a smaller extent: neat MOF-5 pellets densified from 0.3 to 0.7 g/cm^3 exhibit a doubling of conductivity from 0.07 to 0.14 W/m K.

These and other studies have shown that variations in processing and composition can significantly alter materials properties [17,18]. For example, uni-axial compression has been linked to the formation of microstructural anisotropy in compacted ENG [19]. Similarly, the addition of high-aspect-ratio particles to a matrix phase can lead to anisotropic behavior [20] [21]. These observations suggest that MOF/ENG pellets could also exhibit anisotropic thermal transport arising from a combination of uni-axial compression and worm-like ENG additions.

The existence of anisotropic thermal transport could impact the design and operation of an adsorbent-based gas storage vessel. For example, consider a storage system that employs a stack of densified MOF "pucks." The heat-exchanging manifold for this design could consist of circular plates sandwiched between puck faces. In this case it is desirable to maximize transfer along the axial direction of the pucks to/from the heat exchanging plates. Alternatively, for a cylindrical shell heat exchanger in contact with the rims of the pucks, facile transport along the radial direction of the pucks is desirable. These scenarios demonstrate that quantifying (and controlling) the degree of thermal anisotropy is an important consideration when processing the storage media. Nevertheless, one should recognize that densification and ENG additions generally reduce the gravimetric capacity of the storage medium [9,13–15]. Therefore the tradeoff between improved thermal transport and lower capacity should be carefully considered.

The present study examines the possibility for anisotropic thermal transport in uni-axially compressed MOF/ENG composites using thermal conductivity measurements and microstructural characterization on the prototype compound, MOF-5. Due to its high gas storage capacity and simple crystal structure, MOF-5 is perhaps the most widely studied MOF. It is comprised of 1, 4-benzenedicarboxylate (BDC) organic linkers and Zn_4O tetrahedral clusters, the latter serving as secondary building units. MOF-5 can adsorb a large amount of hydrogen, up to 7.1 excess wt.% at 77 K and 40 bar [22]; recent studies have also suggested promising performance for natural gas storage [23]. In addition to its high gravimetric capacity, recent analysis by Goldsmith, et al. indicated that MOF-5 is one of a small number of MOFs that also exhibits high volumetric gas storage densities [24].

In the present study we demonstrate that the high-aspect ratio morphology of second-phase ENG additions, combined with uni-axial compression, results in anisotropic microstructural and thermal transport properties in composite MOF-5/ENG particles. Microscopy of pellet cross-sections confirms the presence of a textured microstructure having MOF particle boundaries and ENG orientations perpendicular to the pressing direction. Thermal conductivity data spanning from cryogenic to ambient temperatures reveal that the values perpendicular to the pressing direction are 2 to 4 times higher than in the pressing direction. We furthermore demonstrate that this anisotropy can be exploited using two straightforward processing techniques. First, a custom die/compression geometry allows for reorientation of the preferred heat flow path. Secondly, fabrication of a layered microstructure with alternating MOF-5 and ENG layers results in an order of magnitude increase in thermal conductivity, at the expense of only minor ENG additions (5 wt.%). These data suggest that the magnitude and preferred direction for thermal transport in MOF compacts may be tuned by altering the processing conditions and nature of the second-phase additions.

2. Experimental procedure

2.1. Materials preparation

MOF-5 powder was provided by BASF, and was synthesised using a process described previously [14]. Expanded natural graphite, ENG, was provided by SGL Group. Synthesis of ENG proceeds by soaking natural graphite flakes in sulfuric acid, followed by heating at 700 °C for 12–15 min to remove acid residues [19,25]. MOF-5 and ENG powders are shown in Fig. 1. MOF-5 powders are white in color, and are composed of small, cubic particles with diameters ranging from 0.1 to 1.5 mm [14]. In turn, each MOF particle is comprised of individual crystallites with diameters in the range of 0.2 to 3 μm [Fig. 1b]. The diameter of the interparticle voids is typically several microns. Images of ENG powder are shown in the lower panel of Fig. 1c, d. ENG consists of relatively large black vermicular particles ranging in length from approximately 0.5 to 4 mm. The density of ENG (~0.1 g/cm^3) is approximately 20 times smaller than normal graphite (2.25 g/cm^3) [25]. The worm-like structure of the ENG arises from the expansion of natural graphite's lamellar structure. ENG particles exhibit a high aspect ratio (length/diameter), ranging from 18 to 25 [26].

2.1.1. Pellets with homogeneous ENG distribution

Pellets formed in the laboratory and at a pilot-plant (BASF) were synthesised and characterized. (See Section 1 in the Supporting Information for details regarding pellets formed using the pilot-plant approach.) Lab-scale pellets were formed using MOF-5 powder and a fractional mass of ENG (weighed on a digital scale) needed to achieve a desired ENG weight percent (0%, 5% and 10%). A SPEX 8000 M Mixer/Mill was filled with the two powders and shaken in the milling machine for 20 s without milling balls. The MOF-5/ENG blends were subsequently loaded into punches and dies with different bore diameters and shapes. Specimens were compressed using a manual pellet press (Reflex Analytical), which was housed inside an Ar-filled glovebox. Cylindrical and rectangular shaped pellets were formed and characterized (Fig. 2a,c). Cylindrical samples were used for microstructure characterization and room temperature thermal diffusivity measurements; rectangular samples were primarily used for steady-state heat flow thermal conductivity measurements, where a rectangular geometry best accommodates the size of the stainless-steel contacts of the instrument. To examine the impact of compression direction, two different types of die were designed for each sample shape. In the case of the cylindrical geometry, this allowed for pellets to be processed using uniaxial compression along either the radial or axial directions (Fig. 5). Likewise, for the rectangular geometries, compression was performed parallel, or perpendicular to, the long axis of the pellet (Fig. 7; also see Section 4 in the Supporting Information).

2.1.2. Pellets with layered ENG distribution

As an alternative to mixing MOF-5 powder with ENG before compression, pellets with a layered MOF-5/ENG microstructure were also fabricated. In this case cylindrical pellets were made using radial pressing (Fig. 5c). Before compression, known masses of pure MOF-5 and ENG were separated according to the desired ENG composition fraction, and then divided into several parts. These parts were then added into the die alternatively and pressed

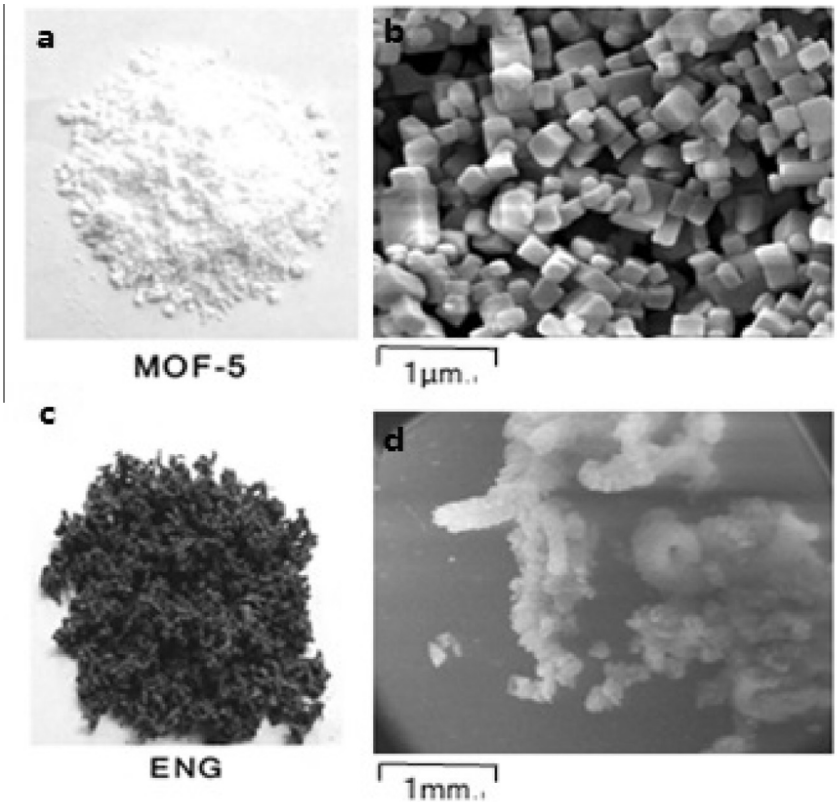

Fig. 1. Images of MOF-5 (upper panel) and ENG powders (lower panel).

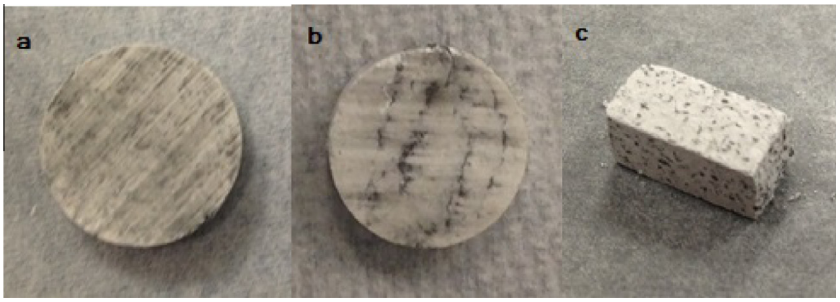

Fig. 2. Cylindrical and rectangular MOF-5/ENG composite pellets. (a, b) Cylindrical pellet used for room temperature measurements and microstructure characterization. Pellet diameter = 1.28 cm, thickness = 3 mm, density = 0.4 g/cm^3. The pellet in (a) has a homogeneous ENG distribution, while the pellet in (b) has a layered ENG distribution. (c) Rectangular sample used for low-temperature measurements (80 – 300 K). The sample dimensions are 10 × 5 × 5 mm. Sample density = 0.35 g/cm^3.

into pellet form. A pellet containing four ENG layers is shown in Fig. 2b.

2.2. Materials characterization

2.2.1. Microscopy

Optical [Olympus SZX12 model 2.2.0 (x90) & Nikon microphot-FXA (x1000)] and scanning electron microscopy (JEOL 6610, FEI Quanta 3D SEM/FIB, and Phillips XL30FEG) were used to investigate the microstructure of MOF-5 compacts. Pellets were cross-sectioned to observe the inter-particle boundaries and the orientation and distribution of ENG. Images were collected using Image-PRO Plus software and analyzed using ImageJ software. Scanning electron microscopy was used to conduct energy dispersive spectroscopy of the sample (Supporting Information, Figure S3). In order to reduce surface charging, the beam current was reduced, low vacuum mode was used, and/or the sample was coated with either silver (Ag) or gold (Au). Images and composition maps from the SEM were collected using either the AZTEC EDS system or the EDAX Genesis system. ImageJ [27] was used to quantify the orientation relationship of the ENG particles with respect to the pressing direction in order to characterize the impact of pressing direction on ENG alignment.

2.2.2. Room temperature thermal conductivity

The room temperature thermal conductivity κ was determined using a transient method for measuring the thermal diffusivity, combined with the following equation:

$$\kappa = \alpha \cdot C_p \cdot \rho. \quad (1)$$

Eq. (1) [28] is a standard expression derived from the transient heat transport equation: $\frac{\partial T}{\partial t} = \alpha \nabla^2 T$. Here α is the thermal diffusivity, which is a function of the thermal conductivity, κ, sample density, ρ, and specific heat capacity c_p: $\alpha = \kappa/(\rho \cdot c_p)$. The parameters κ, ρ, c_p (and therefore α) are temperature dependent, and were determined over the temperature range of interest, 25–65 °C. ρ is

determined using the pellet's external dimensions and mass. C_p measurements were performed on 6.35 mm pellets with a differential scanning calorimeter (DSC) (SENSYS DSC, Setaram), which was calibrated with a sapphire standard. Pellets were placed inside an alumina crucible while being handled inside an Ar-filled glovebox, and then transferred to the DSC (external to the glovebox). Data were collected using a heating rate of 5 °C/min and a He carrier gas flow of 20 ml/s.

Thermal diffusivity measurements at room temperature and above were performed using a xenon thermal flash diffusivity instrument (Anter Flashline, FL3000S2) with N_2 as a protective gas, and with pellets having a 12.8 mm diameter and 3 mm average thickness (Fig. 2a). In this method the temperature of the rear surface of the sample is measured as a function of time after a laser pulse with known power is shined on the sample's opposite surface. The method of Clark and Taylor [29], which accounts for heat loss of the sample during the measurement, was used to estimate the thermal diffusivity. The instrument was calibrated using an iron standard. A thin copper sheet was applied to the top surfaces to prevent the pellets from fracturing during measurement due to the temperature probes, and silver paint was used to adhere the copper to the sample surface. Graphite was coated on the lower surface of the pellet to improve light absorption. Before measurement, the pellets were evacuated at room temperature for at least 3 h. Two measurements were taken for each pellet at the following temperatures: 25 °C, 35 °C, 45 °C, 55 °C, and 65 °C. Notice that for this measurement technique the heat flow is along the axial direction of the pellet. It is therefore possible to characterize anisotropies in thermal conductivity by performing measurements on pellets pressed in distinct (i.e., axial or radial) directions. For pellets pressed axially (as described further below), the thermal flash sample geometry results in a heat flux which is largely perpendicular to the average ENG orientation (Fig. 5a,b), Conversely, pellets pressed radially exhibit ENG orientations more closely aligned with the heat flow direction (Fig. 5c).

The transient method compliments the steady-state method (described below) in that it provides reliable thermal conductivity data at room temperature and above. At these temperatures losses due to thermal radiation can be significant, leading to complications in the use of the steady-state technique.

2.2.3. Low-temperature thermal conductivity

The low-temperature thermal conductivity was measured in the temperature range of 80 to 300 K using a steady-state comparative method that is well-suited for materials having low thermal conductivity [30]. In contrast to the transient method, which requires measurement of both the thermal diffusivity and specific heat capacity, the steady state method directly measures the thermal conductivity using the dimensional Fourier law. This approach is more convenient at cryogenic temperatures. A rectangular-shaped sample with a cross section of 5 mm × 5 mm and length of 3 mm was sandwiched between two stainless-steel contacts (SS304) with the same cross section and thickness of 10 mm (initial attempts employed a longer sample with typical length of 10 mm. However, the radiation losses associated with a sample of this size led to poor estimates of the thermal conductivity. The temperature-dependent thermal conductivity of the stainless-steel contacts have been previously measured [31]. Stycast epoxy was used to mount the sample to the steel contact as well as reduce the contact resistance, and did not permeate the samples. A strain gauge heater was mounted on top of one steel contact, while the other contact (placed under the sample) was connected to the heat sink, thereby generating a heat flux from the top of the pellet to the bottom [32,33].

Measurements were conducted in vacuum to prevent parasitic convection and adsorption within the MOF pores. Two copper cylinders were mounted outside the cold finger as radiation shields. The temperature of the sample holder was controlled by a Lakeshore 340 temperature controller. Six thermocouples (TC1–TC6) were inserted into small-bore holes in the top (TC1, TC2) and bottom (TC5, TC6) steel plates and affixed to the top and bottom of the sample (TC3, TC4) [see Supporting Information, Section 5]. These probes were used to determine the heat fluxes through the steel contacts (TC5, TC6, TC1, and TC2) and the temperature drop across the sample (TC3, TC4) upon heating, from which the sample's thermal conductivity was derived. The sample's thermal conductivity κ was determined using the 1D Fourier law:

$$\kappa = \frac{Q \cdot t_s}{A_s(T_3 - T_4)}, \tag{2}$$

where t_s and As are the sample thickness and cross-sectional area, and Q is the power through the sample. Q was estimated using the power $A_b\ k_b\ (T_5\text{-}T_6)/t_b$ transferred through the bottom steel plate, where k_b is the thermal conductivity of the steel contact and t_b is the distance between TC5 and TC6. T_3, T_4, T_5, T_6 are the temperatures measured using the thermocouples TC3, TC4, TC5 and TC6, respectively. A_b and t_b are the thickness and cross-sectional area of the bottom steel contact, respectively. Three major sources of error are associated with Q: uncertainty due to parasitic blackbody radiation losses from the sample, uncertainty due to parasitic conduction losses through the thermocouples, and uncertainty in t_b due to the nonzero thermocouple diameter. Uncertainty in t_s due to surface roughness, uncertainties in temperature and voltage measurements, and the interfacial temperature drops at each end of the sample also contribute to the error. Accounting for the above sources of uncertainty, we estimate the maximum error in the thermal conductivity to be 18%. Since the same bottom steel contact was used for all measurements (fixing t_b), the relative uncertainty in thermal conductivity for the two samples is less than 9%.

3. Results and discussion

3.1. Pellets with homogeneous ENG distribution

3.1.1. Microstructure

Fig. 3a shows an optical microscopy image for a representative MOF-5 particle after milling with 5 wt.% ENG. Here the MOF-5 appears as a large white particle, and the ENG as black, rod-shaped particles adhered to the MOF surface. As the initial particle size of ENG is typically much larger than that of MOF-5, yet the particles depicted in Fig. 3 suggest that ENG is smaller, we infer that some fracture of the ENG worms occurs during milling. An SEM image of the interface between an ENG particle and a MOF-5 particle in a MOF-5/ENG pellet is shown in Fig. 3b. The compacted MOF-5 powder retains its cubic morphology with crystallite diameters less than 1 μm. The interface contains regions exhibiting good contact between the MOF and ENG, interspersed between gaps or pores. The ENG particle itself retains a layered or parallel sheet structure as previously identified [34]. The preservation of the ENG's lamellar graphite structure suggests that the high thermal conductivity of the original ENG is maintained within the ENG particles.

The distribution of ENG within the MOF-5/ENG pellets was quantified by analyzing optical micrographs of pellet cross sections. Inspection of the cross-sectioned pellets revealed the presence of dark lines connecting ENG deposits. At higher magnifications these lines were shown to contain ENG particles, which appear to collect in the spaces between the MOF-5 conglomerates during compression Fig. 4a, b. Pellets comprised of neat MOF-5 did not show features similar to those of Fig. 4.

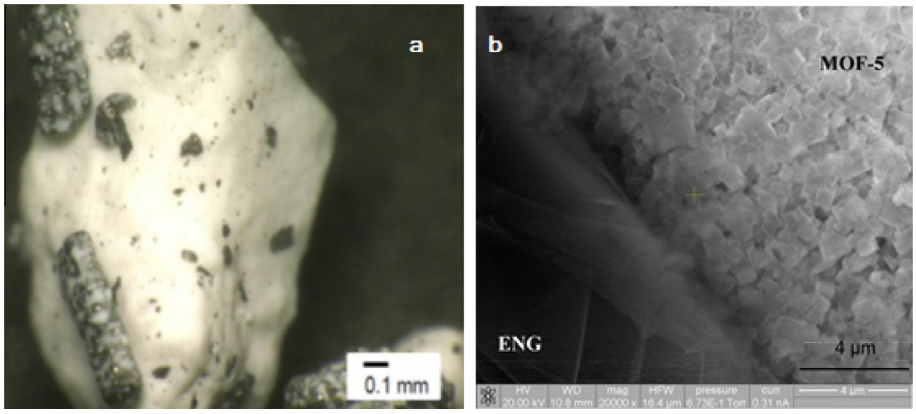

Fig. 3. (a) Optical microscopy image of MOF-5 particles (white) coated with ENG (black) after milling. (b) SEM of the interface between MOF-5 and ENG within a densified pellet containing 5 wt.% ENG and with a pellet density = 0.50 g/cm^3.

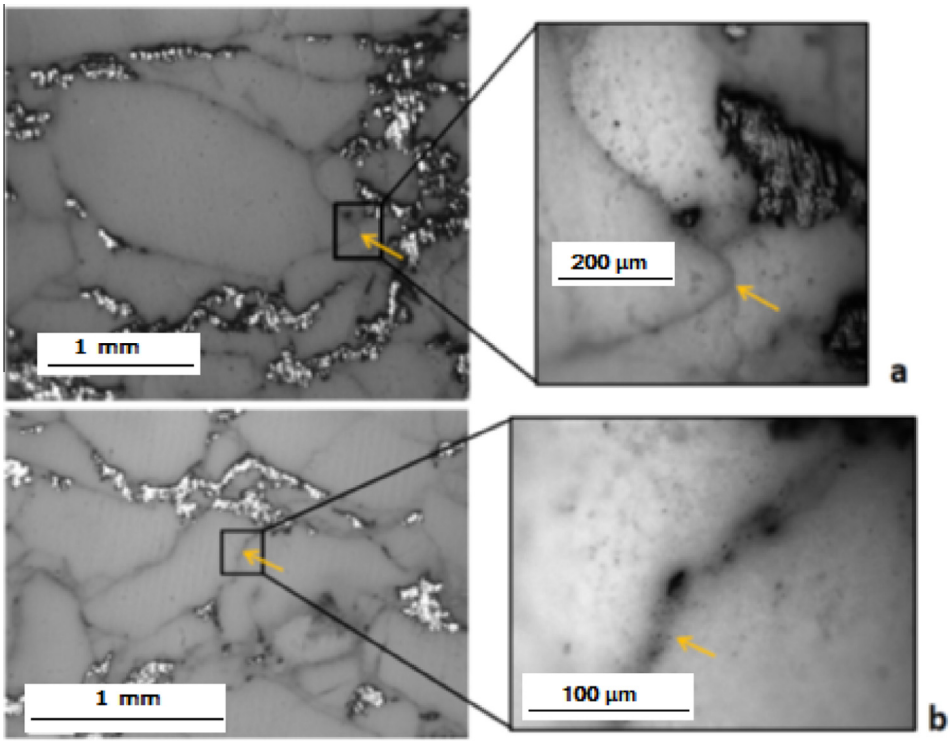

Fig. 4. Cross sections of MOF-5 pellets containing 5 wt.% ENG and with density of 0.38 g/cc imaged using optical microscopy. The images depict boundary lines consisting of ENG deposits at (a) magnifications of x50 and x200 as well as at (b) x50 and x400.

Fig. 5 shows micrographs of cross sections for three pellets formed using different pressing directions and amounts of ENG. The pressing direction in Fig. 5a and b is along the axial direction of the pellet, while the pellet in Fig. 5c was pressed radially. The images at the top of Fig. 5 are of cross-sections obtained from cutting the pellet along the rectangular plain shown in the lower sketch. Arrows overlaid on the microscopy images indicate the compression direction.

The relationship between ENG orientation and the pressing direction was calculated using ImageJ image processing software. Table 1 shows the average angle of ENG particles with respect to the compression direction. The average angle of the ENG in all three cases depicted in Fig. 5 is approximately 70 degrees, confirming that the ENG within the pellets has a tendency to align perpendicular to the pressing direction. Such behavior should encourage the formation of a percolating network in directions perpendicular to the pressing direction, resulting in higher thermal conductivity in the same directions (as described below). A similar relationship between the orientation of the ENG particles and pressing direction was observed across all of the pellets examined (14 in total, data not shown).

As shown in Fig. 3, ENG particles tend to adhere to the surface of MOF-5 particles. Upon densification into pellets this surface adhesion results in the ENG populating the boundaries between MOF-5 particles. Consequently, the color differences between MOF-5 (white) and ENG (black), combined with this "interface decoration" effect, can be used to demark the boundaries between MOF-5 particles. As shown in Fig. 5 (top) the boundaries also display an anisotropic texture as a result of uni-axial compression.

3.1.2. Thermal conductivity

To assess the possibility for anisotropic transport, thermal conductivity measurements were performed on pellets synthesised using different compression directions, as previously described.

Table 1
Average orientation and standard deviation of ENG particles in MOF-5/ENG composites with respect to the pressing direction for the three pellets described in Fig. 5: (a) MOF-5 mixed with 5 wt.% ENG, pressed axially; (b) MOF-5 mixed with 10 wt.% ENG, pressed axially; and (c) MOF-5 mixed with 5 wt.% ENG, pressed radially. The solid black segment represents the average orientation of ENG in the pellet. Black arrows and the dashed line represent the pressing direction. The standard deviation refers to the distribution of ENG orientations observed in cross-sectioned pellets.

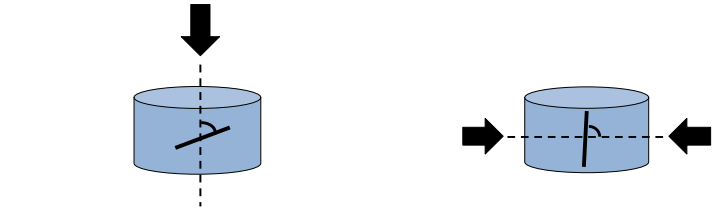

	Sample # from Fig. 5		
	(a)	(b)	(c)
Average orientation of ENG with respect to pressing direction (degrees)	66.3°	69.9°	70.8°
Standard deviation (degrees)	18.6°	17.7°	18.8°

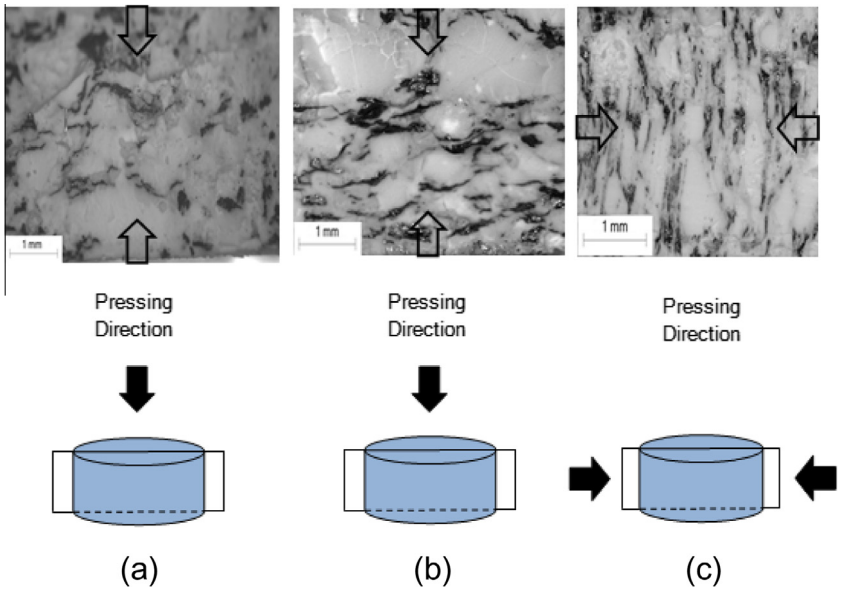

Fig. 5. Cross section of a MOF-5/ENG pellet from optical microscopy. Arrows indicate the pressing direction. The sketch below each image shows the relationship of the cross-section plane to the pressing direction. (a) MOF-5 mixed with 5% ENG, pressed axially; (b) MOF-5 mixed with 10% ENG, pressed axially; and (c) MOF-5 mixed with 5% ENG, pressed radially.

Fig. 6 shows near-ambient temperature thermal conductivity data for MOF-5/ENG pellets having different mass fractions of ENG and orientations of the pressing direction with respect to the direction of heat flow. The error bars in Fig. 6 refer to the range of measured values, and not to the standard deviation. This range may be traced to variations in sample preparation (e.g., related to the distribution of ENG within a given pellet). The data show that the thermal conductivity of the pellet increases in proportion to the ENG weight percent, consistent with our prior findings [13]. For example, at 30 °C the thermal conductivities of pellets containing 0%, 5% and 10% ENG are 0.08, 0.38, and 0.99 W/m K, respectively, for pellets in which the ENG is aligned parallel to the heat flow direction. A similar trend holds for the other ENG orientation and at other temperatures. As expected, the highest conductivity (0.99 W/m K) is found for pellets containing the highest concentration of ENG (10 wt.%), in which the ENG is oriented parallel to the heat flow direction. Conversely, neat MOF-5 pellets have the lowest overall conductivity of less than 0.10 W/m K, and this conductivity is largely independent of the compression direction.

Fig. 6 also illustrates that pellets having the same ENG composition, but different ENG orientations, exhibit differing thermal conductivities. Pellets with ENG orientations parallel to the heat flow (filled symbols) exhibit conductivities that are 2 to 4 times higher than in pellets where the orientation is perpendicular (open symbols). For the ENG concentrations considered here, this anisotropy appears to be independent of the amount of ENG added. Our observation of anisotropic transport in MOF-5/ENG composites is consistent with previous reports involving pellets synthesised from pure ENG [19]. In that case, thermal conductivities of 1.40 and 3.13 W/m K were measured in the axial and radial directions, respectively, consistent with the alignment of vermicular graphite perpendicular to the pressing direction.

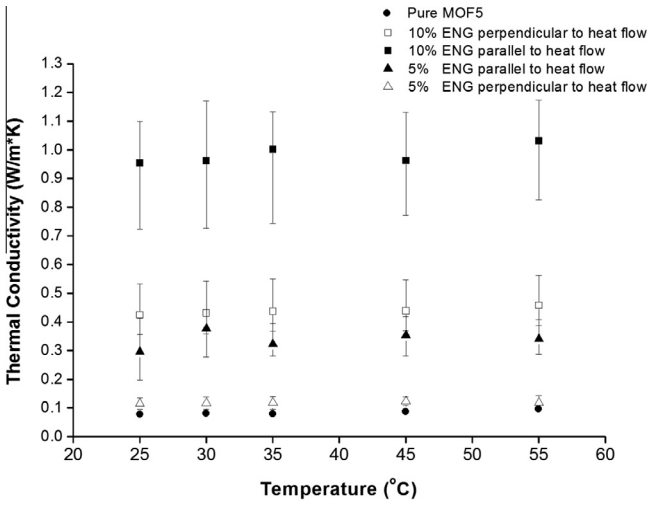

Fig. 6. Near-ambient temperature thermal conductivity for MOF-5/ENG pellets (0.4 g/cm^3) as a function of temperature, ENG content, and pressing direction. Error bars correspond to the range of measured values.

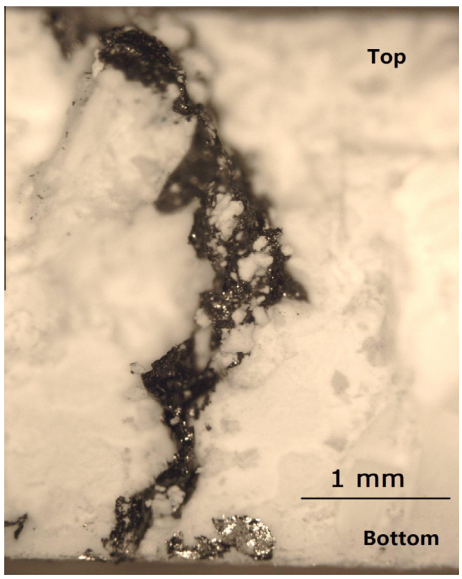

Fig. 8. (Left) Optical microscopy image of a cross-section of a MOF-5 pellet containing ~5 wt.% ENG in a layered distribution. The graph shows the cross section of pellet after being cut perpendicular to the ENG layers; the top and bottom surfaces of pellet are labeled. MOF-5 layers are white, while the ENG layers are black. (Right) Schematics showing the orientation of the ENG layers. The dashed rectangle shows the cross-sectional plane.

Fig. 7 shows the thermal conductivity measured from cryogenic to room temperature (80 K to 300 K). The increasing thermal conductivity at low temperatures (80–200 K) arises from phonon excitations, while the moderate decrease above 200 K is due to a reduction in the average phonon mean free path. The sample having ENG aligned parallel to the heat flow direction (white sample) exhibits the highest value of thermal conductivity 0.68 W/m K. A much lower maximum conductivity is observed 0.17 W/m K in the case of perpendicular ENG alignment. This factor of four improvement in thermal conductivity is consistent with the range we observed for room temperature measurements. These data further signify the presence of significant transport anisotropies arising from ENG orientation and/or MOF-5 boundary effects caused by anisotropic compression.

The differences in room temperature thermal conductivities obtained with the transient and steady-state heat flow method (SSHFM) (0.38 W/m K for the transient method vs. 0.62 W/m K for SSHFM) can be explained by the different sample fabrication and measurement techniques. For example, in the stead-steady state method Black-body radiation losses are expected to have a larger impact at elevated temperatures, leading to some loss in accuracy. These losses are described by the Stefan–Boltzmann law,

$$J = \sigma T^4, \tag{3}$$

where j is the total power radiated per unit area, T is the absolute temperature and $\sigma = 5.67 \times 10^{-8}\ \mathrm{Wm^{-2}K^{-4}}$ is the Stefan–Boltzmann constant. Eq. (3) indicates that radiation at 300 K is 198 times larger than that at 80 K. Therefore the assumption that heat transfer occurs solely via conduction (Eq. (2)) becomes less valid as temperature increases. To minimize the radiation loss across the sample, the length of the sample in Fig. 2c was reduced (by cutting) in order to decrease the heat path length between the two steel contacts. However, the cutting process increases the surface roughness of the pellet, thus introducing uncertainty in t_s in Eq. (2). The Stycast epoxy accumulated in the hollow part of the sample will also contribute to the error of the calculated thermal conductivity. On the other hand, the transient method employs a sample with a very flat surface, as well as Clark and Taylor corrections for radiative losses near room temperature [35], leading us to conclude that the latter method is more reliable at higher temperatures.

3.2. Pellets with layered ENG distribution

3.2.1. Microstructure

We also explored direct manipulation of the ENG distribution as a means to improve the thermal conductivity in a specified direction. In this case we fabricated MOF-5/ENG composite pellets having a microstructure consisting of alternating layers of MOF-5

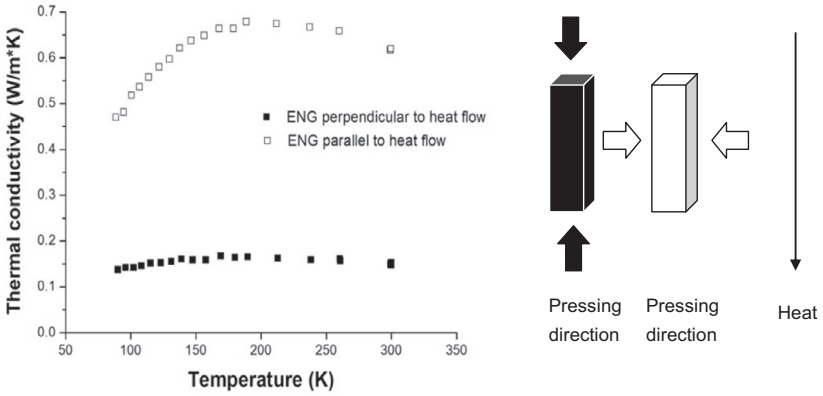

Fig. 7. Thermal conductivity of 0.35 g/cm^3 pellets containing 5% ENG formed using two orthogonal pressing directions over the temperature range of 80–300 K.

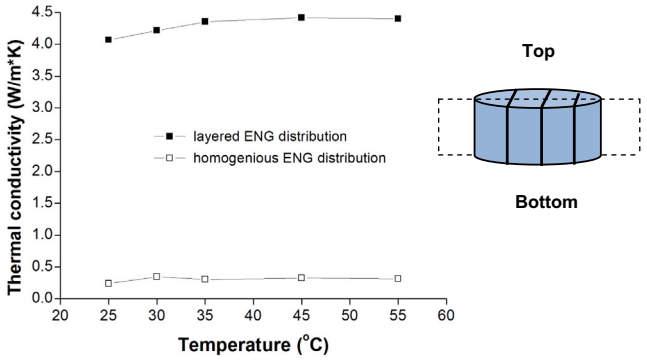

Fig. 9. Thermal conductivity of pellets with two different ENG distributions (layered and homogeneous) at near-ambient temperatures. Both pellets contain approximately 5 wt.% ENG. Layered pellets contain ENG layers (shown schematically at right) which are parallel to the heat flow direction, which is from top to bottom of the pellets. Data for the homogeneous pellets are reproduced from Fig. 5, and refer to the samples identified as "5% ENG parallel to heat flow.".

and ENG. This approach serves as an alternative to the previous approach of tuning the ENG particle orientations via altering the pressing direction. Fig. 8 illustrates the alternating regions of pure MOF-5 (white) and ENG (black) within such a pellet. The pellet contains approximately 5 wt.% ENG distributed amongst 3 separate layers. (The field of view in Fig. 8 contains only one ENG layer.) Each ENG layer traverses the entire thickness of the pellets, connecting the top and bottom surfaces, potentially resulting in a "shorted" heat conduction pathway in the axial direction.

3.2.2. Thermal conductivity

The thermal conductivity of the layered pellet was measured at near-ambient temperatures using the transient method, as shown in Fig. 9 (filled rectangles). The measured value at 35 °C is 4.35 W/m K. In comparison, Fig. 9 also presents the data taken from comparable pellets (filled triangles in Fig. 6) containing 5 wt.% ENG aligned parallel to the (axial) heat flow direction. In the latter case (corresponding to homogeneously distributed ENG), the thermal conductivity was 0.30 W/m K at 35 °C. Therefore, the layered pellet exhibits more than an order of magnitude (~20x) increase in thermal conductivity compared to a pellet having a homogeneous ENG distribution. As previously mentioned, this impressive jump in thermal conductivity can be attributed to the layered microstructure of the pellet. This microstructure provides a very efficient, high thermal conductivity pathway, and does so without requiring an increase in the mass fraction of ENG.

4. Conclusion

Metal organic frameworks exhibit several properties that make them promising candidates for applications in gas capture, gas storage, and catalysis. Nevertheless, the high porosity of MOFs, and their resulting low intrinsic thermal conductivity, can potentially offset these advantages in cases where efficient heat transport is required. In the present study we establish that the high-aspect ratio morphology of second-phase ENG additions, combined with uni-axial compression, results in anisotropic microstructural and thermal transport properties in composite MOF-5/ENG particles. The presence of a textured microstructure having particle boundaries and ENG orientations perpendicular to the pressing direction were confirmed via microscopy of pellet cross-sections. Thermal conductivity measurements ranging from cryogenic to ambient temperatures indicated that heat transport perpendicular to the pressing direction is 2 to 4 times higher than in the pressing direction. Furthermore, we demonstrated that this anisotropy could be exploited using two straightforward processing techniques: First, the preferred heat flow path can be reoriented by use of a custom die/compression geometry. Second, fabrication of a layered microstructure with alternating MOF-5 and ENG layers results in a 20x increase in thermal conductivity, at the expense of only minor ENG additions (5 wt.%). These data suggest that the magnitude and preferred direction for thermal transport in MOF compacts may be tuned by altering the processing conditions and nature of the second-phase additions. We speculate that these techniques could also be effective in tailoring mass transport (permeation) within MOF composites.

Conflict of interest

None declared.

Acknowledgements

The U.S. Department of Energy, Office of Energy Efficiency and Renewable Energy provided primary funding for this study under award number DE-FC36-GO19002. Additional funding for the low-temperature thermal conductivity measurements was provided by the Center for Solar and Thermal Energy Conversion, an Energy Frontier Research Center funded by the U.S. Department of Energy, Office of Science, Basic Energy Sciences under Award # DE-SC-0000957.

Appendix A. Supplementary data

Supplementary data associated with this article can be found, in the online version, at http://dx.doi.org/10.1016/j.ijheatmasstransfer.2014.11.053.

References

[1] J.L.C. Rowsell, O.M. Yaghi, Metal-organic frameworks: a new class of porous materials, Microporous Mesoporous Mater. 73 (1–2) (2004) 3–14.
[2] U. Mueller, M. Schubert, F. Teich, H. Puetter, K. Schierle-Arndt, J. Pastre, Metal-organic frameworks-prospective industrial applications, J. Mater. Chem. 16 (7) (2006) 626–636.
[3] K. Schlichte, T. Kratzke, S. Kaskel, Improved synthesis, thermal stability and catalytic properties of the metal-organic framework compound Cu3(BTC)2, Microporous Mesoporous Mater. 73 (1–2) (2004) 81–88.
[4] O.M. Yaghi, M. O'Keeffe, N.W. Ockwig, H.K. Chae, M. Eddaoudi, J. Kim, Reticular synthesis and the design of new materials, Nature 423 (6941) (2003) 705–714.
[5] L.J. Murray, M. Dinca, J.R. Long, Hydrogen storage in metal-organic frameworks, Chem. Soc. Rev. 38 (5) (2009) 1294–1314.
[6] T.A. Makal, J.-R. Li, W. Lu, H.-C. Zhou, Methane storage in advanced porous materials, Chem. Soc. Rev. 41 (23) (2012) 7761–7779.
[7] S. Keskin, T.M. van Heest, D.S. Sholl, Can metal-organic framework materials play a useful role in large-scale carbon dioxide separations?, ChemSusChem 3 (8) (2010) 879–891
[8] B. Schmitz, U. Müller, N. Trukhan, M. Schubert, G. Férey, M. Hirscher, Heat of adsorption for hydrogen in microporous high-surface-area materials, ChemPhysChem 9 (15) (2008) 2181–2184.
[9] J. Purewal, D. Liu, A. Sudik, M. Veenstra, J. Yang, S. Maurer, U. Müller, D.J. Siegel, Improved Hydrogen Storage and Thermal Conductivity in High-Density MOF-5 Composites, J. Phys. Chem. C 116 (38) (2012) 20199–20212.
[10] http://www.hydrogen.energy.gov/pdfs/review11/st006_van_hassel_2011_o.pdf.
[11] B.L. Huang, A.J.H. McGaughey, M. Kaviany, Thermal conductivity of metal-organic framework 5 (MOF-5): Part I. Molecular dynamics simulations, Int. J. Heat Mass Transfer 50 (3–4) (2007) 393–404.
[12] B.L. Huang, Z. Ni, A. Millward, A.J.H. McGaughey, C. Uher, M. Kaviany, O. Yaghi, Thermal conductivity of a metal-organic framework (MOF-5): Part II. Measurement, Int. J. Heat Mass Transfer 50 (3–4) (2007) 405–411.
[13] D. Liu, J.J. Purewal, J. Yang, A. Sudik, S. Maurer, U. Mueller, J. Ni, D.J. Siegel, MOF-5 composites exhibiting improved thermal conductivity, Int. J. Hydrogen Energy 37 (7) (2012) 6109–6117.
[14] Y. Ming, J. Purewal, D.a. Liu, A. Sudik, C. Xu, J. Yang, M. Veenstra, K. Rhodes, R. Soltis, J. Warner, M. Gaab, U. Müller, D.J. Siegel, Thermophysical properties of MOF-5 powders, Microporous Mesoporous Mater. 185 (0) (2014) 235–244.
[15] J.J. Purewal, D. Liu, J. Yang, A. Sudik, D.J. Siegel, S. Maurer, U. Müller, Increased volumetric hydrogen uptake of MOF-5 by powder densification, Int. J. Hydrogen Energy 37 (3) (2012) 2723–2727.
[16] A. Rodríguez Sánchez, H.-P. Klein, M. Groll, Expanded graphite as heat transfer matrix in metal hydride beds, Int. J. Hydrogen Energy 28 (5) (2003) 515–527.

[17] L. Lian, F. Ma, H. Zheng, D. Yang, K. Xu, Effect of Uniaxial Strain on Heat Capacity and Thermal Conductivity of Graphene Nanoribbons Passivated by Hydrogen, Integr. Ferroelectr. 144 (1) (2013) 101–106.
[18] D.C. Venerus, D.N. Kolev, Anisotropic thermal conductivity in cross-linked polybutadienes subjected to uniaxial elongation, Macromolecules 42 (7) (2009) 2594–2598.
[19] L.W. Wang, Z. Tamainot-Telto, S.J. Metcalf, R.E. Critoph, R.Z. Wang, Anisotropic thermal conductivity and permeability of compacted expanded natural graphite, Appl. Thermal Eng. 30 (13) (2010) 1805–1811.
[20] A.M. Marconnet, N. Yamamoto, M.A. Panzer, B.L. Wardle, K.E. Goodson, Thermal conduction in aligned carbon nanotube-polymer nanocomposites with high packing density, ACS Nano 5 (6) (2011) 4818–4825.
[21] V.V. Ganesh, N. Chawla, Effect of particle orientation anisotropy on the tensile behavior of metal matrix composites: experiments and microstructure-based simulation, Mater. Sci. Eng. A 391 (1–2) (2005) 342–353.
[22] S.S. Kaye, A. Dailly, O.M. Yaghi, J.R. Long, Impact of preparation and handling on the hydrogen storage properties of Zn4O(1,4-benzenedicarboxylate)3 (MOF-5), J. Am. Chem. Soc. 129 (46) (2007) 14176–14177.
[23] M.K. Rana, H.S. Koh, H. Zuberi, D.J. Siegel, Methane storage in metal-substituted metal-organic frameworks: thermodynamics, usable capacity, and the impact of enhanced binding sites, J. Phys. Chem. C 118 (6) (2014) 2929–2942.
[24] J. Goldsmith, A.G. Wong-Foy, M.J. Cafarella, D.J. Siegel, Theoretical limits of hydrogen storage in metal-organic frameworks: opportunities and trade-offs, Chem. Mater. 25 (16) (2013) 3373–3382.
[25] http://www.sglgroup.com/cms/_common/downloads/products/product-groups/eg/construction-materials-ecophit/ECOPHIT_G_e.pdf.
[26] A. Celzard, J.F. Marêché, G. Furdin, Surface area of compressed expanded graphite, Carbon 40 (14) (2002) 2713–2718.
[27] Rasband, W.S., ImageJ, U. S. National Institutes of Health, Bethesda, Maryland, USA, http://imagej.nih.gov/ij/, 1997-2014.
[28] J.R. Cannon, The one-dimensional heat equation, in: Encycl. Math. Appl. 23, first ed., Addison-Wesley Publishing Company/Cambridge University Press, 1984. pp. XXV+483..
[29] L.M. Clark, R.E. Taylor, Radiation loss in flash method for thermal-diffusivity, J. Appl. Phys. 46 (2) (1975) 714–719.
[30] J. Hone, M. Whitney, C. Piskoti, A. Zettl, Thermal conductivity of single-walled carbon nanotubes, Phys. Rev. B 59 (4) (1999) R2514–R2516.
[31] T. Ashworth, David R. Smith, Thermal Conductivity 18, in, 1985.
[32] H. Chi, C. Chen, J.D. Phillips, C. Uher, Transport properties of ZnTe: N thin films, Appl. Phys. Lett. 103 (4) (2013).
[33] K.J. Zhang, A. Yadav, K.H. Kim, Y. Oh, M.F. Islam, C. Uher, K.P. Pipe, Thermal and electrical transport in ultralow density single-walled carbon nanotube networks, Adv. Mater. 25 (21) (2013) 2926–2931.
[34] Y.F. Zhao, M. Xiao, S.J. Wang, X.C. Ge, Y.Z. Meng, Preparation and properties of electrically conductive PPS/expanded graphite nanocomposites, Compos. Sci. Technol. 67 (11–12) (2007) 2528–2534.
[35] L.M. Clark Iii, R.E. Taylor, Radiation loss in the flash method for thermal diffusivity, J. Appl. Phys. 46 (2) (1975) 714–719.